GEO-to-GEO Optical Sensors: Estimating the Detection Rate of Uncataloged Objects

James R. Shell, Ph.D.
Novarum Tech, LLC
Colorado Springs, CO 80908

ABSTRACT

The GEO debris environment remains ill-characterized, hindering best-practices for the long-term stewardship and sustainment of this unique orbital regime. Current ground-based and LEO-based sensing of GEO limits the minimum cataloged object size to approximately one meter, comprising some 1000 objects today. However, statistical surveys by ground-based telescopes continue to affirm a significant population of small objects. The United State space object catalog only contains debris attributed to two GEO fragmentation events; however, many estimate that ten or more GEO fragmentation events have transpired. Further complicating the small debris estimates are wide-ranging assumptions on fragmentation event kinematics, and the extent to which the NASA breakup model applies. However, new efforts may enable GEO-hosted optical sensors, thus providing an opportunity for empirical examination of the small debris population. These potential missions beg the question of exactly what will be "seen" from such payloads. Will the exponentially increasing debris population (with decreasing object size) flood such sensors with many detection events due to the many small objects at relatively short ranges? Or, will the angular rates and required distances sufficient for detection largely preclude their detection? A physics-based model is employed to estimate detection events given an optical payload with a parameterized estimate of the GEO small debris environment. It is found that only for the most aggressive small debris population estimates that small objects dominate detections. Object sizes on the order of 10 cm and larger are found to comprise the majority of detection events.

1 INTRODUCTION

In-situ GEO optical sensors enable an opportunity to sense the small GEO debris population, thus providing a unique means to better quantify the population of GEO orbital debris otherwise not detectable. Candidate GEO missions which may enable GEO-based sensing include satellite servicing[1] and commercially-hosted payloads[2]. A critical question for these candidate missions: what should be anticipated for the detection rate of uncataloged objects? Will the close range afforded by such sensors result in a flood of detections due to populous small debris; and how might the detections be used to further enhance the understanding of the GEO debris population? In order to address these questions, a parametric model is employed to explore the anticipated detections given various assumptions of the debris population and sensor performance.

First, the current understanding of the GEO debris population is reviewed (Section 2), where an emphasis is placed on a means to provide a range of estimates for the smaller (< 30 cm) debris population. Next, an expression is developed for the spatial density of GEO debris objects as a function of size (Section 3), followed by determining the sensing volume of candidate sensors (Section 4). This provides the debris population eligible for sensing, which is turned into actual detections by incorporating the sensor sensitivity, ranges and angular rates of debris objects, all of which interplay with the optical system detection performance (Section 5). Finally, two candidate sensor classes are examined, and the resulting detections are summarized.

2 GEO DEBRIS POPULATION

There are currently some 1000 GEO space objects down to a size ~1 meter maintained by the US Space Surveillance Network. The International Scientific Optical Network (ISON), using a more expansive definition of "GEO" claims to maintain more than 1700 GEO objects.[3] However, it is the much smaller and correspondingly the more populous object sizes that need to be understood in order to estimate GEO-based sensor detections.

In the early 1990s, the increasing availability of CCDs enabled new capabilities for ground-based telescopes to survey GEO debris. A NASA-led initiative from 1992-1994 provided early indications of a significant population of uncataloged GEO objects, likely attributed to unknown fragmentation events.[4] Additional surveys conducted under sponsorship of NASA[5] and the European Space Agency[6] confirmed the uncataloged population, and the bimodal distribution of detection events as a function of visual magnitude. Noteworthy in these surveys was the discovery of a class of objects[7] with high area-to-mass ratios, termed HAMR objects, which presumably originate from thermal control blankets.[8] Continued GEO surveys by NASA primarily using the MODEST telescope provided statistical measurement of the GEO debris population down to 30 cm in size. These statistical observations were consistent with the NASA Standard Breakup Model,[9] and formed the basis of extrapolating the GEO debris population down to 10 cm.[10] The results indicated that at 10 cm and greater, there are more than 3000 objects in GEO.[11] Subsequent optical surveys by more capable systems such as Pan-STARRS have been completed (ref Figure 1), but the results not yet integrated to update the ca2007 NASA population estimates down to 10 cm.

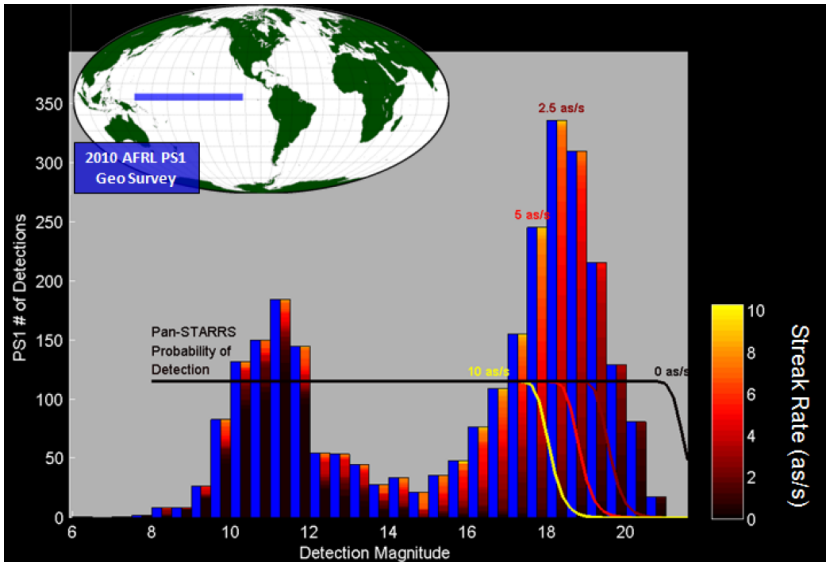

Figure 1 The small debris population as sampled by the Pan-STARRS. An increasing debris population with decreasing size is observed, up to the sensitivity roll-off of the system. Used with permission from Bolden.[12]

From 1997 to 2000, the European Space Agency (ESA) flew an impact sensor termed GORID on the Russian Express-2 communications satellite, providing *in situ* measurement of GEO particles on the order of 1 micrometer in size.[13] Although the results had some ambiguity, more detection events were observed than anticipated, and "clusters" of detection events were identified. [14] These results in part formed the basis of ESA's MASTER-2005 debris model, which predicts more than 1 x 10^{14} GEO region particles 1 micrometer and larger. Even higher populations of micron-sized particles have been postulated by Drolshagen based upon material degradation.[15]

So, what is the minimum object size that should be included for uncorrelated detections? It is noted that a 0.1 mm (100 µm) diameter sphere at 70 meters presents a signature of 6 m_v under the typical assumptions of a 90° solar phase angle with 20% diffuse reflectance (ref Figure 2)-or bright enough to be visible to the naked eye. However, objects of this size and smaller inherently have increasing area to mass ratios. The net result is a relatively limited lifetime in the GEO region given the solar radiation pressure perturbations. A significant outflow from degrading materials would be required to sustain a meaningful population resident in the GEO region.[16] As such, a lower size limit of 0.1 mm will be considered in this analysis.*

* Note a 0.1 mm diameter aluminum sphere has an area to mass ratio of 5.36 m^2/kg.

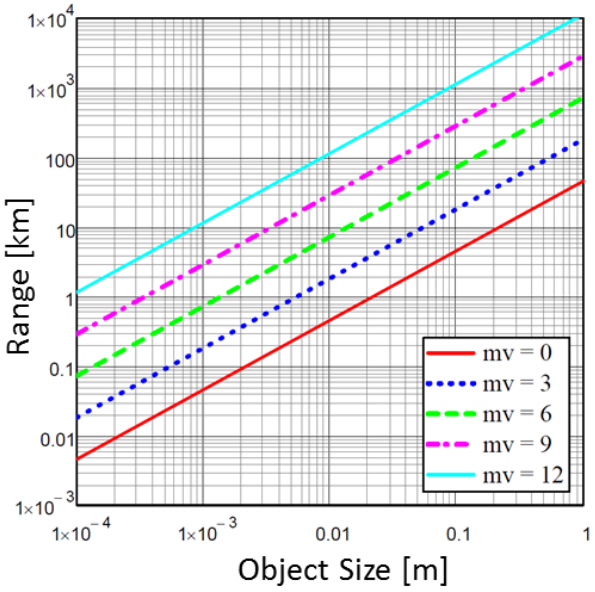

Figure 2 The visual magnitude of a diffuse sphere as a function of range and object diameter (size) under the assumption of a 90° solar phase angle with 20% diffuse reflectance.

One means of representing the number of small debris objects is via a power law representation. In this formulation, the cumulative number of objects, *N*, having size greater than *d* follows the function form of

$$N = Cd^{x} \tag{1}$$

where *C* is a scaling coefficient, and *x* is the slope. This power law relationship will be employed as the means to parameterize the small debris population numbers for this investigation.

For high and low intensity explosions, such as that from upper stages, NASA determined the population scales according to $C = 6$ and $x = -1.6$, specifically being valid for upper stages with masses of 600-1000 kg.[17] For this study, a scaling coefficient of 100 is used, providing an approximate fit to the number of objects 10 cm and larger anticipated. This value is also reasonable given the likely number of fragmentation events which have occurred in GEO, but not explicitly identified. For a higher estimate of debris objects, a slope of -2.8 is used, with a scaling coefficient of 10. This roughly follows ESA's MASTER-2005 debris model. Figure 3 illustrates these two equations and the resulting total number of GEO objects. A "low" debris estimate is also made, using $C = 400$ and $x = -0.87$.

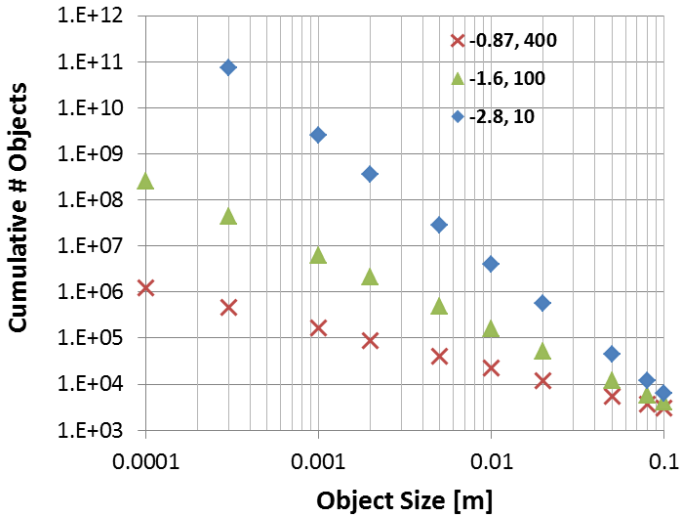

Figure 3 The cumulative number of GEO debris objects as a function of size as modeled by the power law relationship with varying scaling coefficients and slopes. The ESA MASTER 2005 model roughly follows that of the blue diamonds (slope of -2.8), while the green triangles are more representative of the NASA breakup model (slope of -1.6).

3 GEO OBJECT SPATIAL DENSITY

Prior to determining estimates for the GEO object spatial density, one must first define the GEO region. For the purposes of this paper, the GEO region is that populated by active or formerly active geosynchronous satellites and their debris. Therefore the super synchronous disposal orbits are included, along with higher inclination objects resulting from natural solar-lunar perturbations, or inclinations up to approximately 15 degrees for typical area to mass ratio objects. To ensure the inclusion of small fragmentation debris with adequate area to mass ratios (and hence durable lifetimes in the GEO region), the GEO altitude ± 1500 km is considered as the approximate volume containing such objects based upon fragmentation ejection velocities predicted by the NASA breakup model. However, this altitude range is maintained as a variable to explore the resulting density changes and hence detection rate impacts.

The resulting GEO region volume is then calculated as the product of *i*) the GEO orbit circumference (42158 km x 2pi), *ii*) the GEO height of 15° inclination (2 x sin(15°) x 42158 km) and *iii*) the range extent of 3000 km (± 1500 km above and below), producing a total volume of some 1.72 x 10^{22} m^3. Within this volume, a simplifying assumption is made that the objects are uniformly distributed. While this assumption is known to be incorrect, it is deemed sufficient to understand the mean behavior. For instance, it is known that higher densities of objects exist around the geopotential wells, having varying oscillation periods. Furthermore, solar-lunar perturbations produce the familiar inclination/RAAN synchronization of objects. While these localized temporal and spatial effects will impact specific detection occurrences, a uniform distribution assumption provides meaningful detection statistics.

The resulting spatial density is therefore the total number of GEO objects as predicted by the varying cumulative debris object power law, divided by the total GEO region volume.

4 SENSING VOLUME

Optical sensors having a rectangular field of view (FOV) are considered. The volume enveloped by a rectangular FOV sensor increases as a function of range, *R*, and according to the fields of view of the two sensor axis. The volume such a sensor intercepts is given by

$$V = \frac{4}{3} R^3 \arcsin\left[\sin\left(\frac{x_{FOV}}{2}\right)\sin\left(\frac{y_{FOV}}{2}\right)\right] \tag{2}$$

where x_{FOV} and y_{FOV} are the fields of view of the respective sensor axes. The sensors are assumed to be resident on geostationary satellites such that their inclinations are maintained near zero and that the optical axis is oriented along the orbital plane. Modifications to this volume equations are made for instances in which the FOV exceeds an eligible region which may be occupied by debris. For instance, when the y-axis FOV (or "north-south") exceeds the inclination range limit of an object, that volume is no longer eligible to contain lower inclination objects.

The product of the sensing volume, coupled with the object spatial density as a function of size thus provides the number of eligible objects which are within the FOV of a sensor. Having established this object population as the candidates for detection, the nuances of "detectability" are investigated.

5 QUANTIFYING DETECTION EVENTS

To quantify detection events, an absolute radiometry model is not employed. Such models and sensitivity estimation techniques are well-describes elsewhere,[18] and sensitivity as a function of optical system design parameters are not explicitly needed in this investigation. Rather, a sensor baseline is chosen which has a stated capability, and the detection performance is analyzed by examining those variables which impact detection performance.

The optimized detection performance of a fixed staring optical sensor will be considered, operated such that the integration time is matched to the single pixel transit time (or the time to transit the instantaneous field of view or equivalent point spread function diameter, whichever is greater). Under these conditions in a background-limited case, the signal-to-noise ratio for detection is proportional to the aperture irradiance (E) divided by the square root of the angular rate of the object relative to the sensor, ω. Furthermore, the aperture irradiance is inversely proportional to the range squared, or

$$SNR \propto \frac{E}{\sqrt{\omega}} \propto \frac{(d/R)^2}{\sqrt{\omega}}. \tag{3}$$

The angular rate of the debris object, ω, is determined as it transits the equatorial plane of the earth, or the zero declination position (which would be crossing the center of the optical axis).

The angular rate is determined by first developing an expression for the absolute velocity or "north south" velocity, Vel_{NS}, of such objects relative to a geostationary object is given by

$$Vel_{NS} = \frac{2\pi \cdot inc \cdot a}{P}, \tag{4}$$

where inc is the object inclination, a is the semi-major axis, and P is the orbital period. The resulting angular rate is obtained by dividing the velocity by the range, or

$$\omega = \frac{Vel_{NS}}{R}. \tag{5}$$

The angular rates as a function of inclination for varying ranges are shown in Figure 4. More extensive relative velocity calculations are provided in other references (see Fig 4 in Shell, 2011).[19]

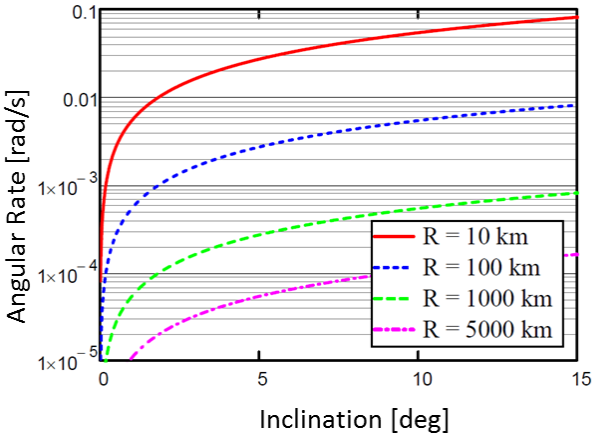

Figure 4 The angular rate of GEO objects as they cross the zero declination position as a function inclination for various ranges from the GEO optical sensor.

By specifying a sensor's detection performance for a particular condition, the performance relative to the other independent variables (object size, range and angular rate) may be parameterized. For instance, if a GEO-hosted sensor can "just" detect a 30 cm object at 1000 km having an inclination of 15° (or the maximum angular rate permissible), then by Equation 3, the SNR is proportional to

$$SNR \propto \frac{(0.1/1x10^6)^2}{\sqrt{802.63/1x10^6}} = C = 1.123x10^{-12}. \tag{6}$$

So for this particular sensor, when other permutations of the variables composed of object size, range and angular rate exceeds the constant, C, of 3.12 x 10^{-12}, then the object may be detected under the optimized integration time assumption. This may be expressed as

$$\text{IF } \frac{(d/R)^2}{\sqrt{\omega}\cdot C} > 1, \text{ THEN detection.} \tag{7}$$

Having developed this expression, the equation may be used to determine the minimum object size detected as a function of the range and angular rate variables, or

$$d_{\min} = R(\sqrt{\omega}\cdot C) = R^{3/4}\cdot Vel^{1/4}\cdot\sqrt{C}. \tag{8}$$

Solving for the maximum range as a function of the object size similarly results in

$$R_{\max} = \left[\frac{d_{\min}}{Vel^{1/4}\cdot\sqrt{C}}\right]^{4/3}. \tag{9}$$

Figure 5 illustrates these equations and shows the relationship between the three independent variables of size, range and angular rate for the point sensor design above.

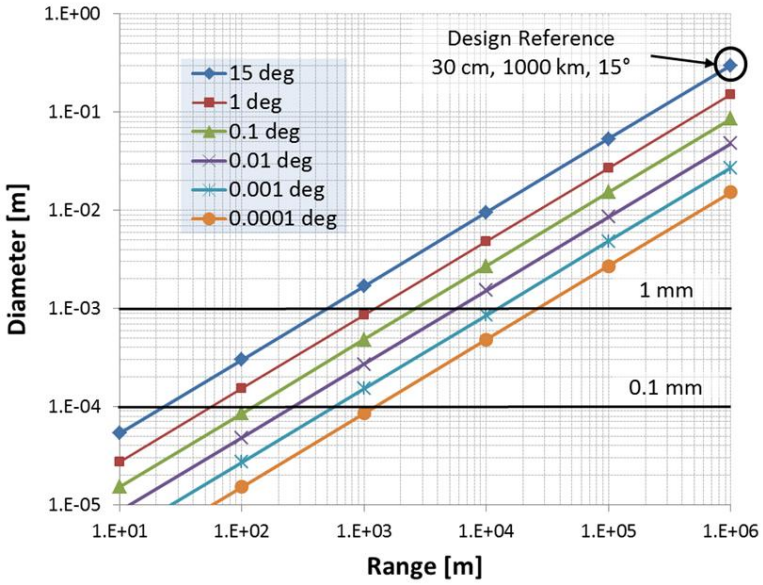

Figure 5 The parameterized detection sensitivity threshold in terms of minimum object size (*y*-axis) and range (*x*-axis) for varying object inclinations (and hence angular rates). Detection is possible for all regions above and to the left of line representing object inclination (or equivalently, angular rate).

With the above framework established, the detection results are obtained in the following a simplistic numerical integration approach. Note the astute mathematician may have success in developing a closed-form solution. The iterative steps to determine the objects detected follow:

1. The object population is determined from the power law relationship with the slope and scaling coefficient (Equation 1).
2. The spatial density of objects are binned according to size and inclinations via uniformly distributing the objects in the GEO volume, with the volume variable according to the extent above and below true GEO
3. The maximum detection range is determined for each of the binned object sizes and inclination ranges (where inclination provides the object angular rate)
4. The maximum detection range is used to calculate the eligible sensor volume according to the object size bin and inclination range (Equation 2), modified by GEO regions the sensor may be intercepting, but not having eligible objects (such looking "above" or "below" low-inclined objects which may never occupy the full volume of the sensor)
5. The detected objects are determined for each imaging frame according to the same object size and inclination bins previously used.

The Appendix contains example tables of the above output to illustrate the flow of results. The final output is provided as the number of detections per imaging frame of the sensor. Two different sensor designs and their results are now examined.

6 RESULTS FOR SENSOR DESIGNS

The detection estimation methodology is now applied to two different notional sensor designs.

6.1 Sensor A: Long Range, Modest FOV

Sensor A is designed to detect 30 cm objects inclined at 15° out to a range of 5000 km, and has a FOV of 10° x 10°. Figure 6 shows the results binned by object sizes using the three debris population assumptions (as shown in Figure 3). For this sensor, the highest debris population model predicts 0.448 detections per random image frame, or approximately one unique object detected every 2 image frames under an assumption that the candidate objects are completely "refreshed" between image frames.

Low # Objects
-0.87 Slope, 400 Coeff

Bins [cm]	Total/Frame
0.01-0.02	1.62E-09
0.02-0.03	2.94E-09
0.03-0.05	1.93E-08
0.05-0.07	3.03E-08
0.07-0.1	8.01E-08
0.1-0.2	1.08E-06
0.2-0.3	1.40E-06
0.3-0.5	6.05E-06
0.5-0.7	7.95E-06
0.7-1.0	1.87E-05
1.0-2.0	2.07E-04
2.0-3.0	2.55E-04
3.0-5.0	1.03E-03
5.0-7.0	1.31E-03
7.0-10.0	2.99E-03
10.0-20.0	3.13E-02
20.0-30.0	3.75E-02
TOTAL	3.72E-02

Medium # Objects
-1.6 Slope, 100 Coeff

Bins [cm]	Total/Frame
0.01-0.02	4.98E-07
0.02-0.03	5.92E-07
0.03-0.05	2.79E-06
0.05-0.07	3.19E-06
0.07-0.1	6.56E-06
0.1-0.2	6.18E-05
0.2-0.3	5.26E-05
0.3-0.5	1.64E-04
0.5-0.7	1.56E-04
0.7-1.0	2.85E-04
1.0-2.0	2.21E-03
2.0-3.0	1.78E-03
3.0-5.0	5.19E-03
5.0-7.0	4.78E-03
7.0-10.0	8.48E-03
10.0-20.0	6.23E-02
20.0-30.0	4.87E-02
TOTAL	8.54E-02

High # Objects
-2.8 Slope, 10 Coeff

Bins [cm]	Total/Frame
0.01-0.02	4.02E-03
0.02-0.03	2.31E-03
0.03-0.05	6.43E-03
0.05-0.07	4.28E-03
0.07-0.1	5.82E-03
0.1-0.2	3.14E-02
0.2-0.3	1.30E-02
0.3-0.5	2.37E-02
0.5-0.7	1.32E-02
0.7-1.0	1.59E-02
1.0-2.0	7.11E-02
2.0-3.0	2.76E-02
3.0-5.0	4.75E-02
5.0-7.0	2.55E-02
7.0-10.0	2.99E-02
10.0-20.0	1.26E-01
20.0-30.0	4.78E-02
TOTAL	4.48E-01

Figure 6 Detection summary for Sensor A, using the "low", "medium" and "high" debris assumptions (left to right), with detection events binned according to object size ranges. (The Appendix contains more detailed calculations for the "high" debris assumption results).

6.2 Sensor B: Short Range, Wide FOV

Sensor B is designed to detect 30 cm objects inclined at 15° out to a range of 1000 km, and has a FOV of 20° x 20°. Figure 7 shows the results binned by object sizes using the three debris population assumptions (as shown in Figure 3). For this sensor, the highest debris population model predicts 0.0255 detections per random image frame, or approximately one unique object detected every 50 image frames under an assumption that the candidate objects are completely "refreshed" between image frames.

Low # Objects
-0.87 Slope, 400 Coeff

Bins [cm]	Total/Frame
0.01-0.02	5.14E-11
0.02-0.03	9.34E-11
0.03-0.05	6.12E-10
0.05-0.07	1.07E-09
0.07-0.1	3.48E-09
0.1-0.2	5.05E-08
0.2-0.3	7.31E-08
0.3-0.5	3.40E-07
0.5-0.7	4.44E-07
0.7-1.0	1.09E-06
1.0-2.0	1.18E-05
2.0-3.0	1.51E-05
3.0-5.0	6.32E-05
5.0-7.0	7.91E-05
7.0-10.0	1.86E-04
10.0-20.0	1.88E-03
20.0-30.0	2.34E-03
TOTAL	2.24E-03

Medium # Objects
-1.6 Slope, 100 Coeff

Bins [cm]	Total/Frame
0.01-0.02	1.58E-08
0.02-0.03	1.88E-08
0.03-0.05	8.88E-08
0.05-0.07	1.12E-07
0.07-0.1	2.85E-07
0.1-0.2	2.90E-06
0.2-0.3	2.74E-06
0.3-0.5	9.19E-06
0.5-0.7	8.72E-06
0.7-1.0	1.66E-05
1.0-2.0	1.26E-04
2.0-3.0	1.05E-04
3.0-5.0	3.18E-04
5.0-7.0	2.89E-04
7.0-10.0	5.28E-04
10.0-20.0	3.74E-03
20.0-30.0	3.04E-03
TOTAL	5.15E-03

High # Objects
-2.8 Slope, 10 Coeff

Bins [cm]	Total/Frame
0.01-0.02	1.28E-04
0.02-0.03	7.35E-05
0.03-0.05	2.04E-04
0.05-0.07	1.50E-04
0.07-0.1	2.53E-04
0.1-0.2	1.47E-03
0.2-0.3	6.76E-04
0.3-0.5	1.33E-03
0.5-0.7	7.37E-04
0.7-1.0	9.32E-04
1.0-2.0	4.03E-03
2.0-3.0	1.64E-03
3.0-5.0	2.91E-03
5.0-7.0	1.54E-03
7.0-10.0	1.86E-03
10.0-20.0	7.58E-03
20.0-30.0	2.98E-03
TOTAL	2.55E-02

Figure 7 Detection summary for Sensor B using the "low", "medium" and "high" debris assumptions (left to right), with detection events binned according to object size ranges.

7 SUMMARY & FUTURE WORK

This simplistic model has enabled a means to estimate the number of uncataloged objects which may be detected by GEO-based optical sensors. While there are many simplifications made, it provides a basis from which empirical results (when obtained) may be interpreted. Most significantly, it appears that even for "high" estimates of the current debris environment, the angular rate/size combination presented to sensors will preclude the detection of

most very small (< 1 cm) debris objects. It is only when the debris power law model slope is less than -3.0 and approaches -4.0 that the very small debris population begins to "overwhelm" the detection events.

The improved understanding of the small GEO debris population will then help inform best practices on use of satellite materials and required disposal techniques to help preserve this orbital regime. Recommended future work includes the incorporation of fixed sensor integration times, and improving the object angular rate determination beyond that of the rates upon GEO orbital plane crossings.

8 APPENDIX

Total Objects Binned by Size and Inclination Ranges										
Size	Inc [deg]									
[cm]	0.001-0.003	0.003-0.01	0.01-0.03	0.03-0.1	0.1-0.3	0.3-1.0	1.0-3.0	3.0-7.0	7.0-15.0	TOTALS
0.01-0.02	1.81E+08	6.33E+08	1.81E+09	6.33E+09	1.81E+10	6.33E+10	1.81E+11	3.62E+11	7.24E+11	1.36E+12
0.02-0.03	2.06E+07	7.21E+07	2.06E+08	7.21E+08	2.06E+09	7.21E+09	2.06E+10	4.12E+10	8.24E+10	1.54E+11
0.03-0.05	7.42E+06	2.60E+07	7.42E+07	2.60E+08	7.42E+08	2.60E+09	7.42E+09	1.48E+10	2.97E+10	5.56E+10
0.05-0.07	1.42E+06	4.98E+06	1.42E+07	4.98E+07	1.42E+08	4.98E+08	1.42E+09	2.85E+09	5.69E+09	1.07E+10
0.07-0.1	5.74E+05	2.01E+06	5.74E+06	2.01E+07	5.74E+07	2.01E+08	5.74E+08	1.15E+09	2.30E+09	4.31E+09
0.1-0.2	2.87E+05	1.00E+06	2.87E+06	1.00E+07	2.87E+07	1.00E+08	2.87E+08	5.74E+08	1.15E+09	2.15E+09
0.2-0.3	3.26E+04	1.14E+05	3.26E+05	1.14E+06	3.26E+06	1.14E+07	3.26E+07	6.53E+07	1.31E+08	2.45E+08
0.3-0.5	1.18E+04	4.11E+04	1.18E+05	4.11E+05	1.18E+06	4.11E+06	1.18E+07	2.35E+07	4.70E+07	8.82E+07
0.5-0.7	2.26E+03	7.90E+03	2.26E+04	7.90E+04	2.26E+05	7.90E+05	2.26E+06	4.51E+06	9.02E+06	1.69E+07
0.7-1.0	9.10E+02	3.19E+03	9.10E+03	3.19E+04	9.10E+04	3.19E+05	9.10E+05	1.82E+06	3.64E+06	6.83E+06
1.0-2.0	4.55E+02	1.59E+03	4.55E+03	1.59E+04	4.55E+04	1.59E+05	4.55E+05	9.09E+05	1.82E+06	3.41E+06
2.0-3.0	5.17E+01	1.81E+02	5.17E+02	1.81E+03	5.17E+03	1.81E+04	5.17E+04	1.03E+05	2.07E+05	3.88E+05
3.0-5.0	1.86E+01	6.52E+01	1.86E+02	6.52E+02	1.86E+03	6.52E+03	1.86E+04	3.73E+04	7.45E+04	1.40E+05
5.0-7.0	3.58E+00	1.25E+01	3.58E+01	1.25E+02	3.58E+02	1.25E+03	3.58E+03	7.15E+03	1.43E+04	2.68E+04
7.0-10.0	1.44E+00	5.05E+00	1.44E+01	5.05E+01	1.44E+02	5.05E+02	1.44E+03	2.89E+03	5.77E+03	1.08E+04
10.0-20.0	7.20E-01	2.52E+00	7.20E+00	2.52E+01	7.20E+01	2.52E+02	7.20E+02	1.44E+03	2.88E+03	5.40E+03
20.0-30.0	8.20E-02	2.87E-01	8.20E-01	2.87E+00	8.20E+00	2.87E+01	8.20E+01	1.64E+02	3.28E+02	6.15E+02
TOTALS	2.11E+08	7.40E+08	2.11E+09	7.40E+09	2.11E+10	7.40E+10	2.11E+11	4.23E+11	8.45E+11	1.58E+12

Figure 8 The total GEO debris population binned according to object size (*y*-axis) and inclination (*x*-axis) using the power law relationship. This example approximates ESA's MASTER-2005 debris model, using a coefficient of 10, with a slope of -2.8 in Equation 1.

Max Range [m]		Inclination [deg]								
		0.001	0.003	0.01	0.03	0.1	0.3	1	3	7
d_min [m]	Bins [cm]	0.001-0.003	0.003-0.01	0.01-0.03	0.03-0.1	0.1-0.3	0.3-1.0	1.0-3.0	3.0-7.0	7.0-15.0
0.0001	0.01-0.02	7.17E+03	4.97E+03	3.33E+03	2.31E+03	1.55E+03	1.07E+03	7.17E+02	4.97E+02	3.75E+02
0.0002	0.02-0.03	1.23E+04	8.54E+03	5.72E+03	3.96E+03	2.65E+03	1.84E+03	1.23E+03	8.54E+02	6.44E+02
0.0003	0.03-0.05	2.43E+04	1.69E+04	1.13E+04	7.83E+03	5.24E+03	3.64E+03	2.43E+03	1.69E+03	1.27E+03
0.0005	0.05-0.07	3.81E+04	2.64E+04	1.77E+04	1.23E+04	8.21E+03	5.70E+03	3.81E+03	2.64E+03	1.99E+03
0.0007	0.07-0.1	6.13E+04	4.25E+04	2.85E+04	1.97E+04	1.32E+04	9.16E+03	6.13E+03	4.25E+03	3.21E+03
0.001	0.1-0.2	1.55E+05	1.07E+05	7.17E+04	4.97E+04	3.33E+04	2.31E+04	1.55E+04	1.07E+04	8.08E+03
0.002	0.2-0.3	2.65E+05	1.84E+05	1.23E+05	8.54E+04	5.72E+04	3.96E+04	2.65E+04	1.84E+04	1.39E+04
0.003	0.3-0.5	5.24E+05	3.64E+05	2.43E+05	1.69E+05	1.13E+05	7.83E+04	5.24E+04	3.64E+04	2.74E+04
0.005	0.5-0.7	8.21E+05	5.70E+05	3.81E+05	2.64E+05	1.77E+05	1.23E+05	8.21E+04	5.70E+04	4.29E+04
0.007	0.7-1.0	1.32E+06	9.16E+05	6.13E+05	4.25E+05	2.85E+05	1.97E+05	1.32E+05	9.16E+04	6.91E+04
0.01	1.0-2.0	3.33E+06	2.31E+06	1.55E+06	1.07E+06	7.17E+05	4.97E+05	3.33E+05	2.31E+05	1.74E+05
0.02	2.0-3.0	5.72E+06	3.96E+06	2.65E+06	1.84E+06	1.23E+06	8.54E+05	5.72E+05	3.96E+05	2.99E+05
0.03	3.0-5.0	1.13E+07	7.83E+06	5.24E+06	3.64E+06	2.43E+06	1.69E+06	1.13E+06	7.83E+05	5.91E+05
0.05	5.0-7.0	1.77E+07	1.23E+07	8.21E+06	5.70E+06	3.81E+06	2.64E+06	1.77E+06	1.23E+06	9.25E+05
0.07	7.0-10.0	2.85E+07	1.97E+07	1.32E+07	9.16E+06	6.13E+06	4.25E+06	2.85E+06	1.97E+06	1.49E+06
0.1	10.0-10.0	7.17E+07	4.97E+07	3.33E+07	2.31E+07	1.55E+07	1.07E+07	7.17E+06	4.97E+06	3.75E+06
0.2	20.0-30.0	1.23E+08	8.54E+07	5.72E+07	3.96E+07	2.65E+07	1.84E+07	1.23E+07	8.54E+06	6.44E+06

Figure 9 The maximum detection range (in meters) is determined according to Equation 8, and solved for according to object size and inclination bin. This example is for a sensor point design capable of detecting a 30 cm object at 5000 km with a 15° inclination.

Vol_Sens [m^3]		Inclination [deg]								
		0.001	0.003	0.01	0.03	0.1	0.3	1	3	7
d_min [m]	Bins [cm]	0.001-0.003	0.003-0.01	0.01-0.03	0.03-0.1	0.1-0.3	0.3-1.0	1.0-3.0	3.0-7.0	7.0-15.0
0.0001	0.01-0.02	3.74E+09	1.25E+09	3.74E+08	1.25E+08	3.74E+07	1.25E+07	3.74E+06	1.25E+06	5.34E+05
0.0002	0.02-0.03	1.89E+10	6.31E+09	1.89E+09	6.31E+08	1.89E+08	6.31E+07	1.89E+07	6.31E+06	2.70E+06
0.0003	0.03-0.05	1.46E+11	4.87E+10	1.46E+10	4.87E+09	1.46E+09	4.87E+08	1.46E+08	4.87E+07	2.09E+07
0.0005	0.05-0.07	4.77E+11	1.87E+11	5.61E+10	1.87E+10	5.61E+09	1.87E+09	5.61E+08	1.87E+08	8.02E+07
0.0007	0.07-0.1	1.37E+12	7.79E+11	2.34E+11	7.79E+10	2.34E+10	7.79E+09	2.34E+09	7.79E+08	3.34E+08
0.001	0.1-0.2	9.11E+12	1.17E+13	3.74E+12	1.25E+12	3.74E+11	1.25E+11	3.74E+10	1.25E+10	5.34E+09
0.002	0.2-0.3	2.70E+13	4.04E+13	1.89E+13	6.31E+12	1.89E+12	6.31E+11	1.89E+11	6.31E+10	2.70E+10
0.003	0.3-0.5	1.06E+14	1.67E+14	1.46E+14	4.87E+13	1.46E+13	4.87E+12	1.46E+12	4.87E+11	2.09E+11
0.005	0.5-0.7	2.60E+14	4.13E+14	4.77E+14	1.87E+14	5.61E+13	1.87E+13	5.61E+12	1.87E+12	8.02E+11
0.007	0.7-1.0	6.72E+14	1.07E+15	1.37E+15	7.79E+14	2.34E+14	7.79E+13	2.34E+13	7.79E+12	3.34E+12
0.01	1.0-2.0	4.27E+15	6.83E+15	9.11E+15	1.17E+16	3.74E+15	1.25E+15	3.74E+14	1.25E+14	5.34E+13
0.02	2.0-3.0	1.26E+16	2.02E+16	2.70E+16	4.04E+16	1.89E+16	6.31E+15	1.89E+15	6.31E+14	2.70E+14
0.03	3.0-5.0	4.91E+16	7.87E+16	1.06E+17	1.67E+17	1.46E+17	4.87E+16	1.46E+16	4.87E+15	2.09E+15
0.05	5.0-7.0	1.20E+17	1.93E+17	2.60E+17	4.13E+17	4.77E+17	1.87E+17	5.61E+16	1.87E+16	8.02E+15
0.07	7.0-10.0	3.12E+17	5.00E+17	6.72E+17	1.07E+18	1.37E+18	7.79E+17	2.34E+17	7.79E+16	3.34E+16
0.1	10.0-20.0	1.98E+18	3.17E+18	4.27E+18	6.83E+18	9.11E+18	1.17E+19	3.74E+18	1.25E+18	5.34E+17
0.2	20.0-30.0	5.84E+18	9.36E+18	1.26E+19	2.02E+19	2.70E+19	4.04E+19	1.89E+19	6.31E+18	2.70E+18

Figure 10 Using the maximum range, the sensor volume available for object detections is determined. Note the pink shaded cells indicate conditions where the sensor volume contains regions where the candidate objects cannot be present, resulting in decreased volume growth with range.

Cum_Objects		Inclination [deg]									
		0.001	0.003	0.01	0.03	0.1	0.3	1	3	7	TOTAL
d_min [m]	Bins [cm]	0.001-0.003	0.003-0.01	0.01-0.03	0.03-0.1	0.1-0.3	0.3-1.0	1.0-3.0	3.0-7.0	7.0-15.0	
0.0001	0.01-0.02	2.60E-03	1.01E-03	2.60E-04	1.01E-04	2.60E-05	1.01E-05	2.60E-06	5.78E-07	2.12E-07	4.02E-03
0.0002	0.02-0.03	1.50E-03	5.83E-04	1.50E-04	5.83E-05	1.50E-05	5.83E-06	1.50E-06	3.33E-07	1.22E-07	2.31E-03
0.0003	0.03-0.05	4.17E-03	1.62E-03	4.17E-04	1.62E-04	4.17E-05	1.62E-05	4.17E-06	9.26E-07	3.40E-07	6.43E-03
0.0005	0.05-0.07	2.61E-03	1.19E-03	3.07E-04	1.19E-04	3.07E-05	1.19E-05	3.07E-06	6.82E-07	2.51E-07	4.28E-03
0.0007	0.07-0.1	3.01E-03	2.01E-03	5.16E-04	2.01E-04	5.16E-05	2.01E-05	5.16E-06	1.15E-06	4.21E-07	5.82E-03
0.001	0.1-0.2	1.00E-02	1.50E-02	4.12E-03	1.60E-03	4.12E-04	1.60E-04	4.12E-05	9.16E-06	3.37E-06	3.14E-02
0.002	0.2-0.3	3.39E-03	5.91E-03	2.38E-03	9.24E-04	2.38E-04	9.24E-05	2.38E-05	5.28E-06	1.94E-06	1.30E-02
0.003	0.3-0.5	4.78E-03	8.78E-03	6.60E-03	2.57E-03	6.60E-04	2.57E-04	6.60E-05	1.47E-05	5.39E-06	2.37E-02
0.005	0.5-0.7	2.25E-03	4.18E-03	4.14E-03	1.89E-03	4.87E-04	1.89E-04	4.87E-05	1.08E-05	3.97E-06	1.32E-02
0.007	0.7-1.0	2.35E-03	4.38E-03	4.78E-03	3.18E-03	8.18E-04	3.18E-04	8.18E-05	1.82E-05	6.68E-06	1.59E-02
0.01	1.0-2.0	7.46E-03	1.39E-02	1.59E-02	2.38E-02	6.54E-03	2.54E-03	6.54E-04	1.45E-04	5.34E-05	7.11E-02
0.02	2.0-3.0	2.50E-03	4.68E-03	5.37E-03	9.37E-03	3.77E-03	1.46E-03	3.77E-04	8.37E-05	3.07E-05	2.76E-02
0.03	3.0-5.0	3.52E-03	6.58E-03	7.57E-03	1.39E-02	1.05E-02	4.07E-03	1.05E-03	2.33E-04	8.54E-05	4.75E-02
0.05	5.0-7.0	1.66E-03	3.10E-03	3.57E-03	6.62E-03	6.56E-03	3.00E-03	7.71E-04	1.71E-04	6.30E-05	2.55E-02
0.07	7.0-10.0	1.73E-03	3.23E-03	3.73E-03	6.95E-03	7.57E-03	5.04E-03	1.30E-03	2.88E-04	1.06E-04	2.99E-02
0.1	10.0-20.0	5.49E-03	1.03E-02	1.18E-02	2.21E-02	2.52E-02	3.78E-02	1.04E-02	2.30E-03	8.46E-04	1.26E-01
0.2	20.0-30.0	1.84E-03	3.44E-03	3.96E-03	7.41E-03	8.52E-03	1.48E-02	5.97E-03	1.33E-03	4.87E-04	4.78E-02
TOTAL		5.91E-02	8.65E-02	7.16E-02	9.36E-02	6.29E-02	5.50E-02	1.48E-02	3.28E-03	1.21E-03	**4.48E-01**

Figure 11 The results are then obtained for a single imaging frame of the sensor, having considered all three variables which impact "detectability" of an object: range, size and angular rate (or inclination equivalent). In the color mapping above, green cells represent more detections, while red fewer. For this case, there are an estimated 0.448 objects which will be detected in each imaging frame of the sensor, with the detections biased toward the relatively larger objects.

9 REFERENCES

[1] DARPA Phoenix Satellite Servicing Web Site, http://www.darpa.mil/Our_Work/TTO/Programs/Phoenix.aspx (accessed 9/2/2013).

[2] James R. Shell, "Commercially-Hosted Payloads for Debris Monitoring and Mission Assurance in GEO," 2011 AMOS Conference, http://www.amostech.com/TechnicalPapers/2011/Orbital_Debris/SHELL.pdf (accessed 9/2/2013)

[3] Igor Molotov, Vladimir Agapov, et al., "Observations with survey instruments of the ISON network," *39th COSPAR Scientific Assembly 2012*, July 14-22, Mysore, India

[4] David L. Talent, Andrew E. Potter and Karl G. Henize, "A Search for Debris in GEO," *Proceedings of the Second European Conference on Space Debris*, Darmstadt, Germany, 17-19 March 1997, ESA SP-393, May 1997. http://adsabs.harvard.edu/abs/1997ESASP.393...99T (accessed 9/2/2013).

[5] K. S. Jarvis, et al., "Charged Coupled Device Debris Telescope Observations of the Geosynchronous Orbital Debris Environment – Observing Year: 1998," NASA/TP-2002-210773, April 2002. http://adsabs.harvard.edu/abs/2002STIN...0248711J (accessed 9/2/2013).

[6] W. Flury, A. Massart, T. Schildknect, et al., "Searching for Small Debris in the Geostationary Ring – Discoveries with the Zeiss 1-metre Telescope," *ESA Bulletin* 104, November 2000. http://www.esa.int/esapub/bulletin/bullet104/flury104.pdf (accessed 9/2/2013).

[7] T. Schildknecht, et al., "Optical Observations of Space Debris in High-Altitude Orbits," *Proceedings of the Fourth European Conference on Space Debris*, Darmstadt, Germany, 18-20 April 2005, ESA SP-587, August 2005. http://adsabs.harvard.edu/abs/2005ESASP.587..113S (accessed 9/2/2013).

[8] J.-C. Liou and J. K. Weaver, "Orbital Dynamics of High Area-to-mass Ratio Debris and Their Distribution in the Geosynchronous Region," *Proceedings of the Fourth European Conference on Space Debris*, Darmstadt, Germany, 18-20 April 2005, ESA SP-587, August 2005. http://adsabs.harvard.edu/abs/2005ESASP.587..285L (accessed 9/2/2013).

[9] N. L. Johnson, P. H. Krisko, et al., "NASA's New Breakup Model of EVOLVE 4.0," *Advances in Space Research*, Volume 28, Issue 9, p. 1377-1384. http://adsabs.harvard.edu/abs/2001AdSpR..28.1377J

[10] P. H. Krisko, et al., "The Geosynchronous Environment for ORDEM 2010," IAC-09-A6.2.02, 2009. http://ntrs.nasa.gov/archive/nasa/casi.ntrs.nasa.gov/20100002022_2009035205.pdf (accessed 9/2/2013).

[11] Nicholas L. Johnson, "Orbital Debris: The Growing Threat to Space Operations," *33rd Annual AAS Guidance and Control Conference*, AAS 10-011, 6-10 Feb 2010.

http://ntrs.nasa.gov/archive/nasa/casi.ntrs.nasa.gov/20100004498_2010003521.pdf (accessed 09/02/2013).

[12] Mark Bolden, Paul Sydney and Paul Kervin, "Pan-STARRS Status and Geo Observation Results," *Advanced Maui Optical and Space Surveillance Technologies Conference*, 2011. http://www.amostech.com/TechnicalPapers/2011/Orbital_Debris/BOLDEN.pdf

[13] Drolshagen, G.; Svedhem, H.; Grün, E., "Measurements of cosmic dust and micro-debris with the GORID impact detector in GEO," *Proceedings of the Third European Conference on Space Debris*, 19 - 21 March 2001. http://adsabs.harvard.edu/abs/2001ESASP.473..177D

[14] A. L. Graps, et al., "GEO Debris and Interplanetary Dust: Fluxes and Charging Behavior," 2006, http://arxiv.org/abs/astro-ph/0609341v1

[15] Drolshagen, et al., "The small size debris population in the GEO belt," *5th European Conference on Space Debris*, 30 Mar – 2 Apr 2009, ESA SP 672, July 2009.

[16] L. Anselmo and C. Pardini, "Orbital Evolution of Geosynchronous Objects with High Area-to-Mass Ratios," *4th European Conference on Space Debris*, 18-20 Apr 2005, ESA SP 587, August 2005.

[17] N. L. Johnson, P. H. Krisko, et al., "NASA's New Breakup Model of EVOLVE 4.0," *Advances in Space Research*, Volume 28, Issue 9, p. 1377-1384. http://adsabs.harvard.edu/abs/2001AdSpR..28.1377J

[18] James R. Shell, "Optimizing Orbital Debris Monitoring with Optical Telescopes," *2010 Advanced Maui and Optical Space Surveillance Technologies Conference*, pp. 427-443. http://www.amostech.com/TechnicalPapers/2010/Systems/Shell.pdf

[19] James R. Shell, "Commercially-Hosted Payloads for Debris Monitoring and Mission Assurance in GEO," 2011 AMOS Conference, http://www.amostech.com/TechnicalPapers/2011/Orbital_Debris/SHELL.pdf (accessed 9/2/2013)